Published in final edited form as:
Magn Reson Imaging. 2009 May ; 27(4): 497–502. doi:10.1016/j.mri.2008.08.001.

Carr-Purcell-Meiboom-Gill (CPMG) Imaging of Prostate Cancer: Quantitative T2 Values for Cancer Discrimination

Joseph R. Roebuck[1], **Steven J. Haker**[1], **Dimitris Mitsouras**[1], **Frank J. Rybicki**[1], **Clare M. Tempany**[1], and **Robert V. Mulkern**[1,2]

[1] Department of Radiology, Brigham and Women's Hospital, Harvard Medical School, 75 Francis St, Boston, MA

[2] Department of Radiology, Children's Hospital, Harvard Medical School, 300 Longwood Avenue, Boston, MA

Abstract

Quantitative, apparent T2 values of suspected prostate cancer and healthy peripheral zone tissue in men with prostate cancer were measured using a Carr-Purcell-Meiboom-Gill (CPMG) imaging sequence in order to assess the cancer discrimination potential of tissue T2 values. The CPMG imaging sequence was used to image the prostates of 18 men with biopsy proven prostate cancer. Whole gland coverage with nominal voxel volumes of $0.54 \times 1.1 \times 4$ mm^3 was obtained in 10.7 minutes, resulting in data sets suitable for generating high quality images with variable T2-weighting and for evaluating quantitative T2 values on a pixel-by-pixel basis. Region-of-interest analysis of suspected healthy peripheral zone tissue and suspected cancer, identified on the basis of both T1- and T2-weighted signal intensities and available histopathology reports, yielded significantly ($p < 0.0001$) longer apparent T2 values in suspected healthy tissue (193 ± 49 ms) *vs*. suspected cancer (100 ± 26 ms), suggesting potential utility of this method as a tissue specific discrimination index for prostate cancer. We conclude that CPMG imaging of the prostate can be performed in reasonable scan times and can provide advantages over T2-weighted fast spin echo imaging alone, including quantitative T2 values for cancer discrimination as well as proton density maps without the point spread function degradation associated with short effective echo time fast spin echo (FSE) sequences.

INTRODUCTION

Prostate cancer is the most common non-cutaneous cancer and the second most common cause of cancer death in American men. In the United States, is has been estimated that 218,890 new cases will be diagnosed and 27,050 men will die of the disease in 2007 (1). Prostate cancer is diagnosed by biopsy, using trans-rectal ultrasound guidance following detection of an elevated prostate serum antigen (PSA) level and/or a suspicious digital rectal examination (2). With a positive diagnosis, prostate cancer patient management decisions are based upon many variables including age, PSA, pathology findings, quality of life, and comorbid illness. It is becoming increasingly apparent that magnetic resonance imaging (MRI) provides valuable information concerning localization of the disease that is useful in the staging process within the framework of the tumor/nodal/metastases (TNM) scoring system (2,3). More specifically, MRI can provide evidence of disease within the prostate, extraglandular extension, involvement of the neurovascular bundles and seminal vesicles, lymphadenopathy in the pelvis

and retroperitoneum, and osseous metastases to the lumbo-sacral spine and bony pelvis. Furthermore, minimally invasive treatment options such as external beam radiation, brachytherapy (4), or focused ultrasound thermal ablation (5) offer alternatives to radical prostatectomy that may be significantly enhanced by using MRI guidance for localizing the disease *in situ*.

Approximately 70% of prostate cancers are found in the peripheral zone (PZ) of the prostate. The primary MR signature of prostate cancer in the PZ is hypointense T2 signal within the normally high signal background from healthy glandular tissue in T2-weighted imaging (3,6–8), as commonly performed with fast spin echo (FSE) sequences. T1-weighted images are also acquired in order to identify areas of hemorrhage from biopsy sites, as these areas have high signal on T1-weighted images and low signal on T2-weighted images which can confound interpretations based on T2-weighted imaging alone (8). The T2-weighted imaging approach has limited specificity and sensitivity (3,6–8), motivating the exploration of additional MR-based techniques to improve the localization of prostate cancer. These include MR-spectroscopic imaging (MRSI) techniques (9–11), diffusion imaging (12–19), quantitative T2 mapping (18–21) and dynamic contrast enhanced (DCE) methods (21,22). In this work, a multi-echo CPMG sequence, performed in a clinically reasonable scan time, is used to generate high quality images of variable T2-weighting. The data is used to construct “apparent” T2 maps that are shown to be of potential utility in discriminating prostate cancer from healthy PZ.

MATERIALS AND METHODS

Patient Selection

A total of 18 treatment naive patients with biopsy-proven prostate adenocarcinoma were recruited for this study and provided written informed consent according to local Institutional Review Board guidelines. The age range was 36 to 75 years (mean 59.7 years). Gleason scores ranged between 3 + 3 = 6 and 4 + 5 = 9 with adenocarcinoma found by biopsy in one or both sides of the prostate in all patients. Three patients were treated with brachytherapy, 3 patients underwent radical prostatectomy, 5 patients were subsequently treated with neoadjuvant chemotherapy prior to radical prostatectomy, and 7 patients were lost to follow up.

MRI Protocol

The examinations were performed using a 1.5 T scanner (General Electric Medical Systems, Waukesha, WI) operating at the 9.1 hardware/software level. An endorectal coil (Medrad, Pittsburg, PA) combined with a four element flexible phased array pelvic coil was used for signal reception. Our standard prostate staging examination was performed on all patients following intramuscular injection of Glucagon 2 mg. Imaging included an axial T1-weighted gradient echo sequence with a repetition time/echo time (TR/TE) of 265/7 ms/ms and an axial T2-weighted fast spin echo (FSE) sequence with TR/TE of 5500/100 ms/ms and echo train length (ETL) of 16. The image matrix (frequency × phase encode)/field-of-view (FOV) and slice-thicknesses for the T1- and T2-weighted imaging sequences were 256 × 128/12 cm/3 mm and 256 × 192/12 cm/3 mm, respectively. Additional T2-weighted FSE sequences in the coronal and sagital planes were obtained using similar parameters to search for seminal vesicle involvement and correlate findings seen on axial T2-FSE images. A second axial T1-weighted gradient echo sequence was performed using a larger FOV and breath-holding to search for retroperitoneal lymph nodes as well as osseous metastases in the lumbo-sacral spine and pelvis. The corresponding acquisition parameters were TR/TE 265/7 ms/ms, image matrix 256 × 160, FOV 36 cm, and slice thickness 5 mm.

In addition to these sequences, a CPMG imaging sequence, created by modifying the manufacturer’s FSE sequence (23,24), was also applied to all patients. The CPMG sequence

utilized the standard slice selective 180° pulses with full phase rewinding in between the refocusing pulses. Applied to the prostate, the CPMG sequence parameters used were TR 2500 ms, echo spacing of 14 ms, ETL of 16, image matrix 256 × 128 (frequency × phase encode), FOV of 14 cm, and a 4 mm slice thickness with a 1 mm gap between slices. The no phase wrap option was employed along the phase encode direction to avoid aliasing at the expense of scan time. With these settings, images were obtained from 8 – 11 slices in either the axial plane (13 cases) or coronal plane (5 cases) in 10.7 minutes with nominal pixel volumes of 0.54 × 1.1 × 4 mm^3.

Image Interpretation and Analysis

Output from the CPMG sequence consisted of 16 single-echo images for each slice with TE values ranging from 14 ms to 224 ms in 14 ms intervals. Post-processing of the zero-filled (256 × 256) magnitude reconstructed images was performed to generate four increasingly T2-weighted images as well as apparent T2 and proton density maps for each slice. The increasingly T2-weighted images were created by bunching the 16 images for each slice into consecutive groups of 4 and calculating the geometric mean of the first, second, third and fourth echo group (*i.e.*, multiplication of each bunch of four consecutive magnitude images followed by fourth root operation). Proton density (ρ) and apparent T2 maps were estimated using pixel-by-pixel fitting of the signals S_i obtained at all echo times TE_i (i = 1,2,3,…,16) to the mono-exponential decay model

$$S_i=\rho\exp(-TE_i/T2), \quad [1]$$

For the T2 values used in the cancer discrimination analyses below, this monoexponential fit was applied only to the first 12 echoes in order to avoid baseline noise contamination. In addition, due to some curvature noted on semi-log plots of signal vs echo time, the T2 decay curves for echoes 2 through 12 were also fit with biexponential functions of the form

$$S=\rho_A\exp(-TEi/T2_A)+\rho_B\exp(-TEi/T2_B) \quad [2]$$

and an F-test comparison (14) was made to determine if the biexponential fits were statistically better than monoexponential fits applied to the same data.

All images were initially reviewed by a blinded reader (RVM) who selected representative regions-of-interest (ROIs) within the PZ by visual inspection and classified them as either suspected healthy (SH) tissue or suspected cancer (SC). The classification of each ROI was based on the signal intensity present in the most heavily T2-weighted geometric mean image (i.e., the 4th echo group). These findings were then reviewed by a radiologist (JRR) and correlated with T1-weighted images to insure that none of the selected ROIs contained hemorrhage and were concordant with available histopathologic diagnosis from core needle biopsy reports (18 cases) and post-radical prostatectomy surgical pathologyreports (3 cases). Direct histopathologic correlation of the these ROIs with the biopsy and/or surgical pathology reports was not possible, however, so that the ROIs employed for analysis, though consistent with biopsy and/or histopathological classification, must be considered regions of normal and abnormal T2 signal as opposed to healthy tissue or cancer per se. At least one SH ROI and one SC ROI were identified for each subject and the T2 value for each ROI was calculated from the corresponding T2 map. A pairwise Student's two-tailed t-test was then used to test for statistical significance of the difference between group mean SH and SC T2 values, with $p <$

0.05 considered significant. Statistical analyses were performed using GraphPad Prism version 3.0 software (GraphPad Software, Inc. San Diego, CA).

RESULTS

High quality diagnostic images with minimal motion artifact were acquired from each patient. Figure 1 shows a representative case taken from an axial slice through the prostate with the geometric mean images generated from the 1st, 2nd, 3rd, and 4th group of TEs together (A–D), and the corresponding T2 (E) and PD (F) maps generated from the full data set. Shown in the 4th group image (D) are representative ROI placements for SH (in blue) and SC (in red). Figure 2 shows data in the same format as Figure 1, but from a coronal data set in a patient with a clearly depicted focal hypointense nodule in the left base. The conspicuity of this lesion varies with the degree of T2-weighting with the greatest conspicuity occurring in the later two geometric mean images. Note how the PD maps from the axial slice (Figure 1F) show shading along the anterior-posterior (AP) direction as a result of the endorectal coil receiver sensitivity profile with respect to the axial slice. In contrast, the coronal PD map (Figure 2F) shows minimal shading, as expected, since this slice was oriented perpendicular to the endorectal coil axis.

Figure 3 presents the T2 values for all the SH and SC ROIs sampled in this study. The mean ± standard deviation of the SH and SC apparent T2 values were 193 ± 49 ms and 100 ± 26 ms, respectively. The difference between the means was statistically significant ($p < 0.0001$). Finally, Figure 4 presents typical T2 decay curve data from one patient, as represented by the natural logarithm of signal intensity *vs.* echo time for the first 12 echoes, for SC and SH ROI's along with baseline noise values measured from an air ROI in the rectum. Two observations are made regarding these decay curves that are characteristic of the T2 decay curves extracted in this study. First, the signal from the first echo was generally found to be less intense than expected, occasionally even less than the second echo, as reported previously using similar CPMG imaging sequences (25). Second, there is a slight curvature of the decay curves on these semilog plots that is indicative of non-monoexponential behaviour (14) from the 2nd echo on. Indeed, biexponential fits to echoes 2 through 12, shown in Figure 4 together with the monoexponential fits, were better representative of the data as verified by F-test comparisons ($p < 0.01$).

DISCUSSION

Treatment options for prostate cancer depend upon many factors including the stage of disease at presentation. Since staging prostate cancer is unreliable with digital rectal examination, PSA, and non-MRI based imaging methods, MRI is becoming an increasingly accepted method in the clinical assessment of men with biopsy-proven prostate cancer. The cornerstone sequence for MRI assessment of the prostate has always been T2-weighted imaging as currently performed with FSE sequences. Due to the collection of k-space lines with variable T2-weightings, there is inevitably some spatial blurring with FSE (23,24,26) which may effect subtle findings critical to staging such as the evaluation of extraglandular extension or involvement of the seminal vesicles. Though our focus is not to quantify the FSE blurring effect on prostate lesion conspicuity, it is a simple fact that T2-filtering effects in k-space leading to spatial blurring are not present when individual lines of k-space are all acquired at a single echo time, as with the CPMG imaging sequence. This lack of blurring, particularly with the PD images generated with the CPMG sequence, may help with prostate cancer staging when used in conjunction with FSE-based sequences applied to other scan planes.

Our primary motivation for using the CPMG imaging sequence was to test the ability to make quantitative measurements of tissue T2 values throughout the gland that may prove of value

in discriminating cancer from healthy tissue, as suggested by the results in Figure 3. Within the context of the limitations of the present study, which include a relatively small set of patients and a necessarily incomplete correlation with histology, the statistically significant difference observed between the mean SC and mean SH values is considered meaningful. Unfortunately there is scant literature with which to compare the actual T2 values measured within SC and SH regions. One early study by Liney et al (20) compared multi-echo vs multiple single echo vs FSE based T2 measurements and reported preliminary T2 values in healthy PZ of around 150 ms but no T2 values for suspected cancerous regions were reported. Engelbrecht et al reported T2 values of 151 ± 89 ms and 331 ± 527 ms for cancerous and non-cancerous PZ, respectively, from a group of 36 patients (21), though the hybrid T2 measurement technique they employed drew criticism (27). Our own group previously reported FSE based T2 measurements in 11 men with prostate cancer and reported SH and SC mean values of 128 ± 43 ms and 103 ± 28 ms, respectively (18). The present study, performed in more men and with a more rigorous T2 measurement technique yielded similar SC values with an even greater separation of SH and SC, 193 ± 49 ms and 100 ± 26 ms, respectively. With a group of 12 prostate cancer patients, Gibbs et al employed FSE based T2 measurements to obtain SH and SC values of 135 ± 40 ms and 82 ± 18 ms (19), grossly similar to our results. Clearly quantitative T2 measurements can provide a more objective measure of underlying tissue properties than signal intensity assessments alone as factors like coil sensitivity and subjective assessments are avoided. Whether the use of quantitative T2 measurements can improve the specificity and/or sensitivity of prostate cancer detection over that available from T2-weighted signal intensity observations alone remains, however, an open and interesting question that requires further study.

Finally, it is important to address the accuracy of the T2 assessments made from the CPMG imaging sequence implemented in this study. The use of slice selective refocusing pulses and phase rewinding is known to lead to errors in T2 measurement due to stimulated echo effects, as discussed by Poon and Henkelman (28). Indeed, these authors have advocated the use of single slice imaging with no phase encode rewinding and non-selective refocusing pulses when truly accurate T2 values are sought. Of course this severely restricts the volume coverage available from a study and, also, is less relevant to the “apparent” T2 values that provide the actual signal intensity observed for T2-weighted FSE sequences. As such, the simple monoexponential T2 values we have extracted are directly relevant to any optimization schemes associated with TE settings in standard FSE sequences, in addition to showing interesting potential for cancer discrimination (Figure 3). The observations of a lower than expected first echo signal intensities and the subtle non-monoexponential behavior, as witnessed by the curvature in the semi-log plots and the improvement afforded by biexponential *vs.* monoexponential fits, may be a consequence of the non-optimal T2 measurement made when slice-selective refocusing pulses and phase encode rewinding is employed. Further studies using the Poon and Henkelman recommendations for true T2 decay curve characterization (28) would be required in order to determine if, in fact, prostate tissues truly exhibit non-monoexponential T2 signal decays as previously found for diffusion decay curves over an extended b-factor range (14).

Acknowledgments

This work was supported in part by NIH 5R25-CA089017, NIH 5RO1CA109246-02 and NIH U41-RRO19703

References

1. Cancer facts and figures. American Cancer Society. 2007. www.cancer.org
2. Presti JC Jr. Prostate cancer: Assessment of risk using digital rectal examination, tumor grade, prostate-specific antigen, and systematic biopsy. Radiol Clin North Am 2000;38:49–58. [PubMed: 10664666]

3. Yu KK, Hricak H. Imaging prostate cancer. Radiol Clin North AM 2000;38:59–85. [PubMed: 10664667]
4. Szot Barnes A, Haker SJ, Mulkern RV, So M, D'Amico AV, Tempany CM. Magnetic resonance spectroscopy-guided transperineal prostate biopsy and brachytherapy for recurrent prostate cancer. Urology 2005;66:1319.e13–1319.e15.
5. Poissonnier L, Chapelon JY, Rouviere O, Curiel L, Bouvier R, Martin X, Dubernard JM, Gelet A. Control of prostate cancer by transrectal HIFU in 227 patients. European Urology 2007;51:381–387. [PubMed: 16857310]
6. Jager GJ, Rijter ETG, van da Kaa C, de la Rosette, Oosterhof GON, Thornbury JR, Barentsz JO. Local staging of prostate cancer with endorectal MR imaging: Correlation with histopathology. AJR 1996;166:845–852. [PubMed: 8610561]
7. Heuck A, Scheidler J, Sommer B, Graser A, Muller-Lisse UG, Massmann J. MR imaging of prostate cancer. Radiologue 2003;43:464–473.
8. White S, Hricak H, Forstner R, Kurhanewicz J, Vigneron DB, Zaloudek CJ, Weiss JM, Narayan P, Carroll PR. Prostate cancer: Effect of postbiopsy hemorrhage on interpretation of MR images. Radiology 1995;195:385–390. [PubMed: 7724756]
9. Scheidler J, Hricak H, Vigneron DB, et al. Prostate cancer: Localization with three-dimensional proton MR spectroscopic imaging-clinicopathologic study. Radiology 1999;213:473–480. [PubMed: 10551229]
10. Van der Graaf M, van den Boogert HJ, Jager GJ, Barentsz JO, Heerschap A. Human prostate: Multisection proton MR spectroscopic imaging with a single spin-echo sequence-preliminary experience. Radiology 1999;213:919–925. [PubMed: 10580976]
11. Zakian KL, Sircar K, Hricak H, Chen H-N, Shukla-Dave A, Eberhardt S, Muruganandham M, Ebora L, Kattan MW, Reuter VE, Scardino PT, Koutcher JA. Correlation of proton MR spectroscopic imaging with Gleason score based on step-section pathologic analysis after radical prostatectomy. Radiology 2005;234:804–814. [PubMed: 15734935]
12. Issa B. In vivo measurement of the apparent diffusion coefficient in normal and malignant prostatic tissues using echo-planar imaging. J Magn Reson Imag 2002;16:196–200.
13. Hosseinzadeh K, Schwarz SD. Endo-rectal diffusion weighted imaging in prostate cancer to differentiate malignant and benign peripheral zone tissue. J Magn Reson Imag 2004:654–661.
14. Mulkern RV, Szot Barnes A, Haker SJ, Rybicki FJ, Maier SE, Tempany CMC. Biexponential characterization of prostate tissue water diffusion decay curves over an extended b-factor range. Magn Reson Imag 2006;24:563–568.
15. Haider MA, van der Kwast TH, Tanguay J, Evans AJ, Hashmi A-T, Lockwood G, Trachtenberg J. Combined T2-weighted and diffusion-weighted MRI for localization of prostate cancer. AJR 2007;189:323–328. [PubMed: 17646457]
16. Shimofusa R, Fujimoto H, Akamata H, Motoori K, Yamamoto S, Ueda T, Ito H. Diffusion-weighted imaging of prostate cancer. J Compu Assist Tomogr 2005;29:149–153.
17. Miao H, Fukatsu H, Ishigaki T. Prostate cancer detection with 3-T MRI: Comparison of diffusion-weighted and T2-weighted imaging. Eur J Radiol 2007;61:297–302. [PubMed: 17085002]
18. Chan I, Wells W III, Mulkern RV, Haker SJ, Zhang J, Zou KH, Maier SE, Tempany CMC. Detection of prostate cancer by integration of line-scan diffusion, T2-mapping and T2-weighted MR imaging; a multi-channel statistical classifier. Med Phys 2003;30:2390–2398. [PubMed: 14528961]
19. Gibbs P, Tozer DJ, Liney GP, Turnbull LW. Comparison of quantitative T2 mapping and diffusion-weighted imaging in the normal and pathologic prostate. Magn Reson Med 2001;46:1054–1058. [PubMed: 11746568]
20. Liney GP, Knowles AJ, Manton DJ, Turnbull LW, Blackband SJ, Horsman A. Comparison of conventional single echo and multi-echo sequences with a fast spin-echo sequence for quantitative T2 mapping: Application to the prostate. J Magn Reson Imag 1996;6:603–607.
21. Engelbrecht MR, Huisman HJ, Laheij RJF, Jager GJ, van Leenders GJLH, Hulsbergen-Van De Kaa CA, de la Rosette JJMCH, Blickman JG, Barentsz JO. Discrimination of prostate cancer from normal peripheral zone and central gland tissue by using dynamic contrast-enhanced MR imaging. Radiology 2003;229:248–254. [PubMed: 12944607]

22. Noworolski SM, Henry RG, Vigneron DB, Kurhanewicz J. Dynamic contrast-enhanced MRI in normal and abnormal prostate tissues as defined by biopsy, MRI, and 3D MRSI. Magn Reson Med 2005;53:249–255. [PubMed: 15678552]

23. Melki PS, Jolesz FA, Mulkern RV. Partial RF echo planar imaging with the FAISE method: I. Experimental and theoretical assessment of artifact. Magn Reson Med 1992;26:328–341. [PubMed: 1513254]

24. Melki PS, Jolesz FA, Mulkern RV. Partial RF echo planar imaging with the FAISE method: II. Contrast equivalence with spin echo sequences. Magn Reson Med 1992;26:342–354. [PubMed: 1513255]

25. Gambarota G, Cairns BE, Berde CB, Mulkern RV. Osmotic effects on the T2-relaxation decay of in vivo muscle. Magn Reson Med 2001;46:592–599. [PubMed: 11550254]

26. Constable RT, Gore JC. The loss of small objects in variable TE imaging: Implications for FSE, RARE, and EPI. Magn Reson Med 1992;28:9–24. [PubMed: 1435225]

27. Mulkern RV, Rybicki FJ, Haker SJ, Tempany CMC. Comments on prostate tissue T2 measurements, Letter to the Editor. Radiology 2004;232:624–625. [PubMed: 15286328]

28. Poon C, Henkelman RM. T2 quantification for clinical applications. J Magn Reson Imag 1992;2:541–553.

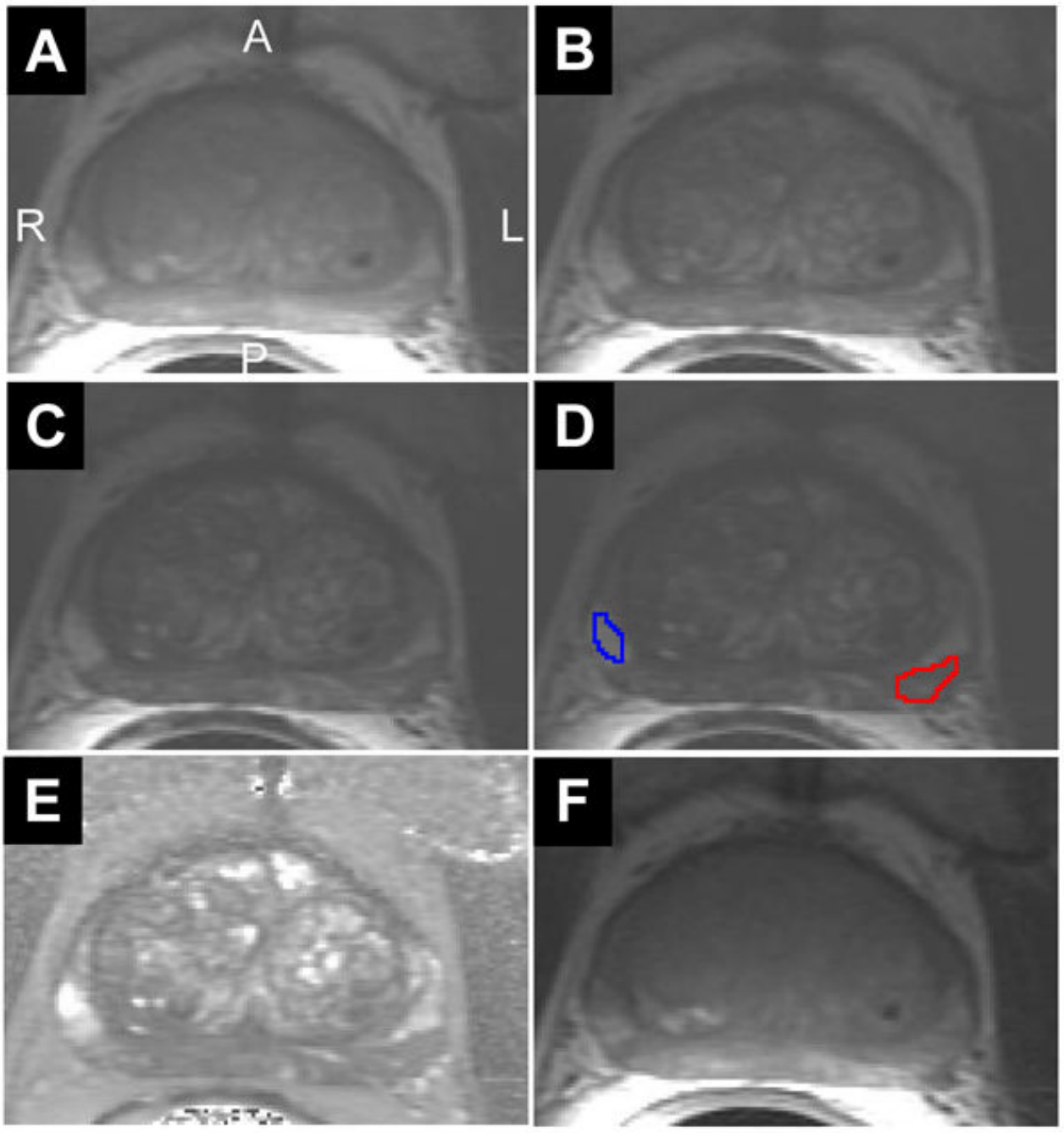

Figure 1.

Axial images of a 63-year old man with biopsy proven prostate adenocarcinoma of the right lobe (Gleason 3+3=6, 5% of 1/3 cores) and left lobe (Gleason 4+3=7, 80%, 20%, and 5% of 3/4 cores) and PSA 7.9 who subsequently underwent radical prostatectomy that showed Gleason 3+4=7 involving the posterior right quadrant and Gleason 3+4=7 involving anterior and posterior left quadrants. Geometric mean images generated from the 1st (**A)**, 2nd (**B)**, 3rd (**C)**, and 4th (**D)** group of TEs. **D** is derived from the last 4 TEs (182, 196, 210, 224 ms) and demonstrates a band of hypointense signal in the posterior right and left midgland but with no evidence of extracapsular penetration (stage T2c). ROI placements for SH (blue) and SC (red)

are shown. **E**. Corresponding T2 map. T2 values for SH and SC were 215ms and 94ms respectively. **F**. Corresponding PD map..

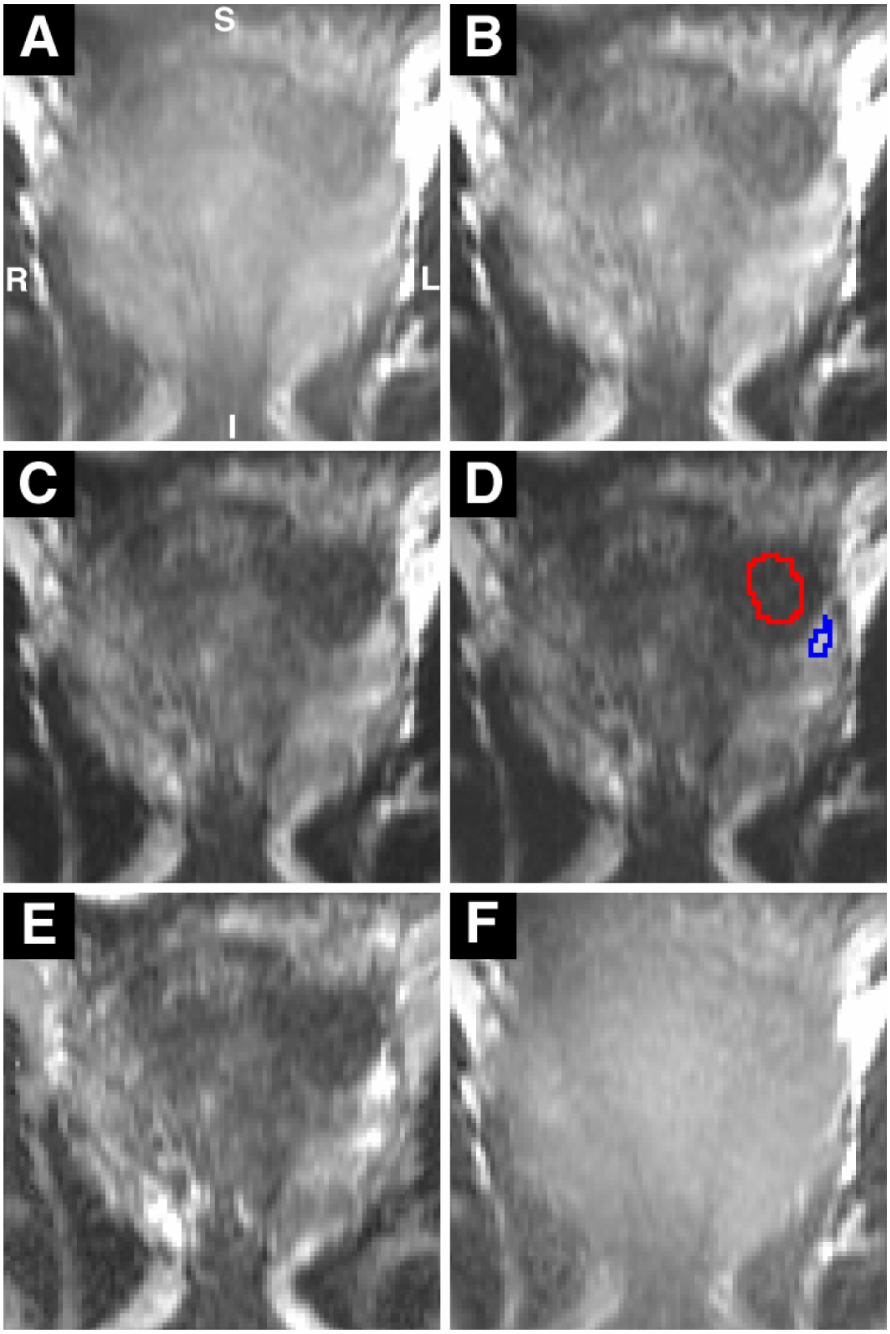

Figure 2.

Coronal images of a 43-year old male with prostate adenocarcinoma of the right lobe (Gleason 4+4=8, 100% and 80% of 2/6 cores) and left lobe (Gleason 4+5=9, 100%, 100%, 100%, and 90% of 6/6 cores) and PSA 41.0 who subsequently underwent neoadjuvant chemotherapy with bevacizumab plus docetaxel prior to radical prostatectomy. Geometric mean images from the 1^{st} – 4^{th} group of TEs (**A**–**D**, respectively). A focal hypointense nodule is noted in the left base that extends beyond the capsule into the left seminal vesicle (stage T3b). ROI placements for SH (blue) and SC (red) are shown. **E**. Corresponding T2 map. T2 values for SH and SC were 195ms and 74ms respectively **F**. Corresponding PD map.

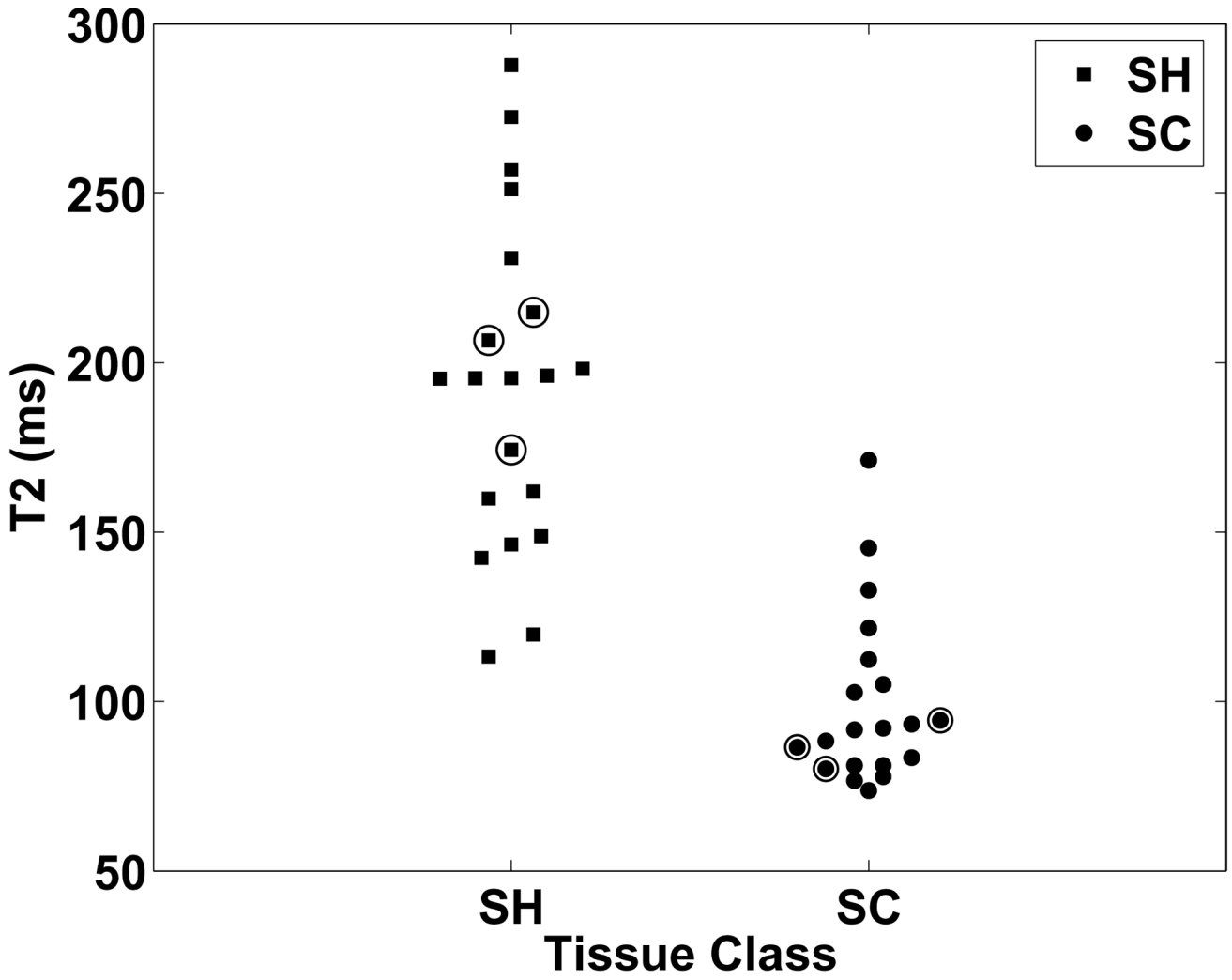

Figure 3.
Apparent T2 values for all suspected healthy (SH) tissue and suspected cancer (SC) peripheral zone ROIs sampled in this study. Three cases in which the patient underwent prostatectomy without first undergoing neoadjuvant therapy are circled. Significant differences were measured between the apparent T2 values of suspected healthy tissue and suspected cancer with $\mu \pm \sigma$ of 193±49 and 100±26 ms, respectively. ($p < 0.0001$)

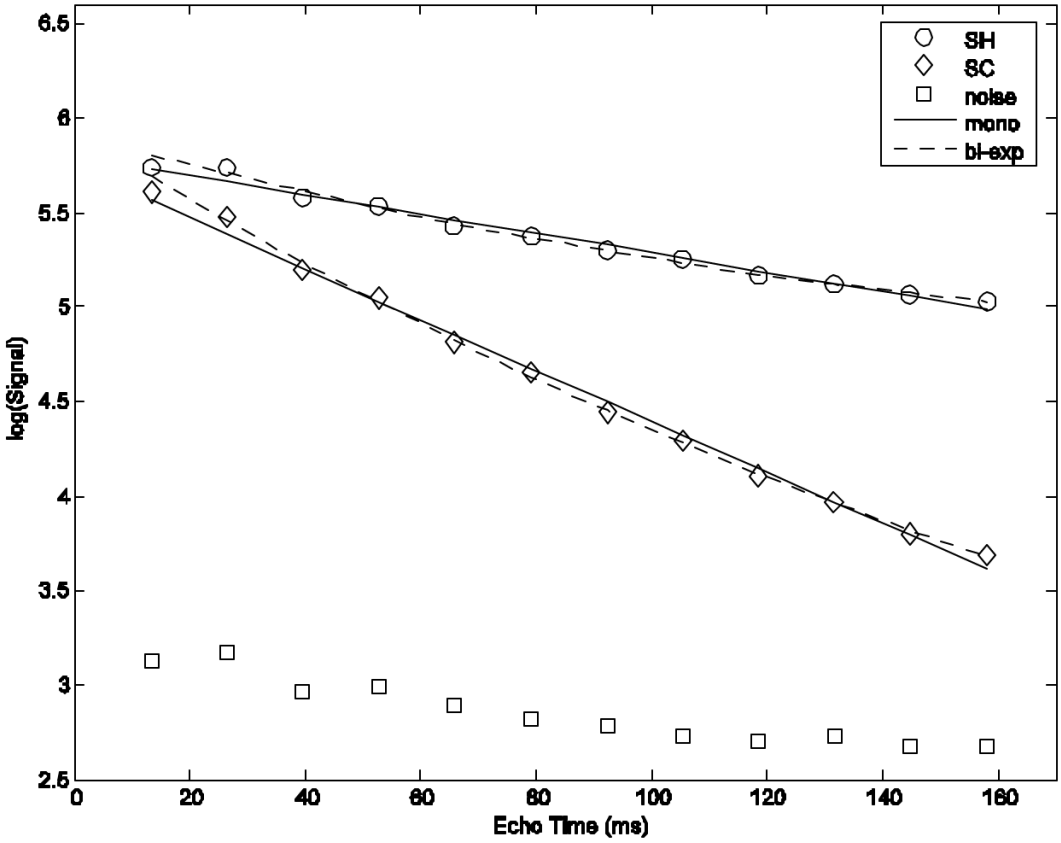

Figure 4.
Typical T2 decay curves with fits to echoes 2 through 12 using mono- and biexponential fits. Note the noise floor is well below the signal remaining in the 12 th echo even for the more quickly decaying SC ROI.